Accurate simulation dynamics of microscopic filaments using "caterpillar" Oseen hydrodynamics

A. G. Bailey,[1,*] C. P. Lowe,[2] I. Pagonabarraga,[3] and M. Cosentino Lagomarsino[4,5]
[1]*Department of Physics, Imperial College London, Exhibition Road, London SW7 2AZ, United Kingdom*
[2]*HIMS, Universiteit van Amsterdam, Nieuwe Achtergracht 166, 1018 WV Amsterdam, The Netherlands*
[3]*Departament de Fisica Fonamental, Universitat de Barcelona, Carrer Marti i Franques 1, 08028 Barcelona, Spain*
[4]*Dipartimento di Fisica, Università degli Studi di Milano, Via Celoria 16, 20133 Milano, Italy*
[5]*INFN, Milano, Via Celoria 16, 20133 Milano, Italy*

(Received 24 April 2009; revised manuscript received 30 July 2009; published 28 October 2009)

Microscopic semiflexible filaments suspended in a viscous fluid are widely encountered in biophysical problems. The classic example is the flagella used by microorganisms to generate propulsion. Simulating the dynamics of these filaments numerically is complicated because of the coupling between the motion of the filament and that of the surrounding fluid. An attractive idea is to simplify this coupling by modeling the fluid motion by using Stokeslets distributed at equal intervals along the model filament. We show that, with an appropriate choice of the hydrodynamic radii, one can recover accurate hydrodynamic behavior of a filament with a finite cross section without requiring an explicit surface. This is true, however, only if the hydrodynamic radii take specific values and that they differ in the parallel and perpendicular directions leading to a caterpillarlike hydrodynamic shape. Having demonstrated this, we use the model to compare with analytic theory of filament deformation and rotation in the small deformation limit. Generalization of the methodology, including application to simulations using the Rotne-Prager tensor, is discussed.

DOI: 10.1103/PhysRevE.80.046707 PACS number(s): 47.11.−j, 87.16.Ka, 05.45.−a, 46.32.+x

I. INTRODUCTION

Microscopic biological filaments moving in a low Reynolds number environment are fundamental to the functioning of organisms. Typical examples include flagella and cilia in the field of microorganism motility [1–3]. Understanding the interplay between the filament and its surroundings has notable biological implications in the context of the incipient stages of life [4] not to mention the design and development of fabricated microswimmers [1,5]. Other biological constituents whose statics and dynamics are critical in cellular function include biopolymers such as microtubules [6,7]. All of these examples have one common feature: the biological component is relatively stiff and has a high aspect ratio (the length greatly exceeding the width). Mechanically these systems exhibit behavior indicative of flexible filaments. The collective complexity of the molecular structure manifests itself simply as an effective bending elasticity. This being the case, one can gain insight by studying inextensible flexible filaments, which serve as a surprisingly good approximation to more realistic descriptions [8].

The interesting counterintuitive behavior of biological systems is often due to the interaction of the body with its viscous environment [1,9,10]. For example, a one-armed swimmer tries to propel itself by waving a stiff appendage, but it will go nowhere in the absence of inertia (low Reynolds number). However, this is a perfectly viable means of propelling one's own body in a swimming pool (high Reynolds number). Resistive force theory [11] is frequently used to mimic this interplay approximating the interaction as a local relationship between the force and velocity. For theoretical investigations, it is useful in that it is more frequently analytically tractable. Hydrodynamic effects, however, are long range and scale inversely with distance rendering this local description quite a limited one. In fact, the very simplest example—a flexible filament in a static external field—yields rich dynamic behavior that is impossible to predict using resistive force theory [10,12,13]. Not surprisingly, incorporating the coupling between the body and the fluid is also significant for more sophisticated systems such as the growth of liquid crystals [14].

With this in mind, here we describe a simple and computationally efficient simulation model of a flexible filament immersed in a viscous fluid. The various force contributions are described in detail. In a simulation, at a small additional computational cost, one is not limited to resistive force theory but can use the more accurate Stokesian description that takes into account the body-fluid coupling. Representing a filament as a sequence of "Stokeslets," or point forces acting on the fluid, is not new [10,12,15,16]; however, we show in this paper that agreement between slender body theory and the continuum limit of the discrete Stokesian hydrodynamic force is conditional on the choice of a tensor hydrodynamic radius with specific values relative to the bead spacing. This is in contrast to previous work where the hydrodynamic radius is set to exactly half of the bead spacing, which is referred to as the "shish kebab" model [17]. We show that by choosing the hydrodynamic radius appropriately, we are not limited to infinitely slender bodies; instead, we can accurately simulate systems that have a realistic aspect ratio such as a flagella which can have a diameter of a few percent of the filament length [2].

II. FILAMENT MODEL

We describe a model filament as a collection of equally spaced points along a curve. All forces and masses are con-

*aimee.bailey06@imperial.ac.uk

centrated at the site locations, which we will refer to as *beads* using conventional nomenclature. Three types of forces—elasticity, hydrodynamics, and tension—form the basis of the model. External forces relevant for a specific application can easily be added.

A. Elastic forces

The filament evolving under elasticity will be penalized for deviation from the lowest energy conformation. If we take the ground state of the elastic filament to be a straight line, the continuous equation for the elastic energy is an integral over the entire contour length of the square of the curvature (κ) [18],

$$U_e = \frac{\alpha}{2}\int_{-l}^{l}\left|\frac{\partial^2 \mathbf{r}}{\partial s^2}\right|^2 ds = \frac{\alpha}{2}\int_{-l}^{l}\kappa^2 ds. \tag{1}$$

The position of the filament is denoted by $\mathbf{r}$. The contour length (s) spans from $-l$ to l, where $L=2l$. The constant α is the elastic flexure or bending rigidity. This result is from continuum elasticity theory but our filament is actually represented as a discrete collection of connected beads separated by a spacing of $b=L/(n-1)$. We introduce the variable θ, which is the deviation of the tangent from the straight line of adjacent segments at bead i given by

$$\cos(\theta_i) = \frac{\mathbf{r}_{i-1,i}\cdot\mathbf{r}_{i,i+1}}{b^2}, \tag{2}$$

where $\mathbf{r}_{ij}=\mathbf{r}_j-\mathbf{r}_i$. Relating the local radius of curvature to the angle θ by the cosine rule, we have

$$\kappa_i^2 = \frac{2}{b^2}[1-\cos(\theta_i)]. \tag{3}$$

Using this relationship, the discrete counterpart of Eq. (1) is

$$U_e = \frac{\alpha}{b}\sum_{i=1}^{n-1}[1-\cos(\theta_i)]. \tag{4}$$

The elastic forces are the gradient of Eq. (4) with respect to position.

In our model the filament has a fixed segment length meaning b is constant (see Sec. II C). Therefore, no elastic energy can be stored in the form of axial extension/compression. The filament simply has an energetic incentive to remain straight. This is analogous to writing Eq. (1) with a Lagrange multiplier term to enforce local length constraints. Experiments measuring force-extension curves indicate the Kratky-Porod wormlike chain model is a good description of biofilaments and proteins [19–22]. Therefore, our combination of a bending penalty plus length constraints is justified.

B. Hydrodynamic forces

In order to mimic the interaction of the filament submersed in a viscous fluid, we need to include hydrodynamic forces. Solving the fluid flow equations exactly with a stick boundary condition in a dynamic simulation, during which the shape evolves, is a computationally daunting task. Alternatively, resistive force theory [11] provides a much simplified description, but there are many instances where one cannot neglect the hydrodynamic coupling [12,14]. Conveniently, we will show that the solution of the flow equations can be approximated by treating the continuous object as a collection of discrete Stokeslets or point forces. At arbitrarily high Stokeslet density, the continuous form of the object is recovered. For example, the hydrodynamic force acting on our filament can be modeled using a line of sufficiently numerous Stokeslets to recreate the behavior of a continuous curve. An advantage of this methodology, in addition to being computationally tractable for simulations over long time scales, is that unbounded geometries can be considered.

The hydrodynamic force in our model is defined by

$$\mathbf{F}_{iH} = -(\gamma_0^{\perp}\hat{\mathbf{n}}\hat{\mathbf{n}} + \gamma_0^{\parallel}\hat{\mathbf{p}}\hat{\mathbf{p}})\cdot(\mathbf{v}_i - \mathbf{v}_{iH}). \tag{5}$$

The vector $\hat{\mathbf{n}}(\hat{\mathbf{p}})$ is the unit direction normal (perpendicular) to the filament. The tensor $\hat{\gamma}_0$ is the bead friction, where $\gamma_0^{\perp(\parallel)}=6\pi\eta a^{\perp(\parallel)}$. The constant η and tensor $\hat{a}$ are the fluid viscosity and the hydrodynamic bead radii, respectively. Note that $\hat{a}$ are not real radii, in that the beads in the model have no spatial extension. Rather, they are parameters dictating the friction strength parallel and perpendicular to the filament axis. The term $\mathbf{v}_i$ is the velocity of the filament at bead i and $\mathbf{v}_{iH}$ is the velocity of the fluid at the same location.

Using the Stokeslet form for the fluid velocity, we have

$$\mathbf{v}_{iH} = \frac{1}{8\pi\eta}\sum_{i\neq j}\left(\frac{\mathbf{F}_j}{|r_{ij}|} + \mathbf{F}_j\cdot\frac{\mathbf{r}_{ij}\mathbf{r}_{ij}}{|r_{ij}|^3}\right), \tag{6}$$

which gives the following hydrodynamic force:

$$\mathbf{F}_{iH} = -(\gamma_0^{\perp}\hat{\mathbf{n}}\hat{\mathbf{n}} + \gamma_0^{\parallel}\hat{\mathbf{p}}\hat{\mathbf{p}})\cdot\left[\mathbf{v}_i - \frac{1}{8\pi\eta}\sum_{i\neq j}\left(\frac{\mathbf{F}_j}{|r_{ij}|} + \mathbf{F}_j\cdot\frac{\mathbf{r}_{ij}\mathbf{r}_{ij}}{|r_{ij}|^3}\right)\right]. \tag{7}$$

$\mathbf{F}_i$ is the force on bead i. Equation (6) is derived by eliminating the convective terms in the Navier-Stokes equations. In other words, it is consistent with the Reynolds number being low, with fluid inertia neglected. In the limit that the force mediated by the fluid is negligible, the hydrodynamic force reduces to resistive force theory with a tensor bead friction,

$$\mathbf{F}_{iH} = -(\gamma_0^{\perp}\hat{\mathbf{n}}\hat{\mathbf{n}} + \gamma_0^{\parallel}\hat{\mathbf{p}}\hat{\mathbf{p}})\cdot\mathbf{v}_i. \tag{8}$$

C. Length constraints

In order to fix the contour length, we use SHAKE methodology to incorporate length constraints in a dynamic simulation [23]. The distance between all connected beads is held at a constant value to within a predefined degree of accuracy. For all results presented here, we set the accuracy to be a relative bead separation $|\mathbf{r}_{ij}|/b$ to within 10^{-12}. Using SHAKE methodology, there is an array of numerical recipes one can use to calculate the Lagrange multipliers that make up the constraint forces. For a linear geometry in which each bead is connected to at most two nearest neighbors, such as

the geometry we are considering here, we use and recommend MILC SHAKE (matrix inverted linearized constraints SHAKE), which can be orders of magnitude faster than SHAKE iteration [24].

D. Integrating the equations of motion

Now that all forces have been identified, what remains to be specified is an appropriate integration scheme to evolve the equations of motion in a dynamic simulation. With velocity-dependent forces present, one cannot use the standard velocity Verlet algorithm [25]. Instead, one can derive an update scheme using the Trotter factorization of the Liouville propagator, the same method used to derive the reversible, multiple time scale, molecular-dynamics scheme reference system propagator algorithms (RESPA) [26]. Furthermore, Kalibaeva *et al.* demonstrated that one can combine a novel update scheme for a particular set of velocity-dependent forces with SHAKE methodology for applying constraints [27]. Details of the procedure can be found in their paper.

Here we use an alternate method to simulate the time evolution of the system. We integrate the bead equation of motion

$$m\frac{d\mathbf{v}_i}{dt} = \mathbf{F}_i, \tag{9}$$

where m is the mass of a single bead and $\mathbf{F}_i$ is the total force (now including the hydrodynamic force) acting on bead i. This is a Langevin equation because the hydrodynamic force can be separated in Eq. (9) into terms that do and do not depend on the velocity

$$m\frac{d\mathbf{v}_i}{dt} = \bar{\mathbf{F}}_i - \gamma_0\mathbf{v}_i. \tag{10}$$

In this section we use a scalar bead friction γ_0 for clarity, although we use the tensor form for our simulation model. Here, the forces $\bar{\mathbf{F}}_i$ are independent of the velocity [including the inhomogeneous part hydrodynamic force; see Eq. (7)]. This being the case, we can rewrite the velocity Verlet algorithm as an implicit scheme for the new velocity. It is

$$\mathbf{r}_i(t+dt) = \mathbf{r}_i(t) + dt\mathbf{v}_i(t) + \frac{dt^2}{2m}\mathbf{F}_i(t),$$

$$\mathbf{v}_i(t+dt) = \frac{2m-\gamma_0 dt}{2m+\gamma_0 dt}\mathbf{v}_i(t) + \frac{dt}{2m+\gamma_0 dt}[\bar{\mathbf{F}}_i(t) + \bar{\mathbf{F}}_i(t+dt)], \tag{11}$$

where dt is the time step. Since we are neglecting inertia in the fluid, the model is only consistent if the inertia of the filament is also negligible. To achieve this we impose the condition that the inertial time scale ($\sim m/\gamma_0$) is very much shorter that all other times scales in the problem. We then verify that the time scales are separated to a sufficient extent that the inertial time does not influence the results. Alternatively, one could directly neglect the inertial term in Eq. (10) prior to integration. The two approaches would yield equivalent results, but we use the present method for facile combination with pre-existing molecular-dynamics code. Further details can be found in Refs. [8,28,29]. Although one could use higher-order methods, we have found this simple integration scheme sufficient and robust. As described here, the simulation model is deterministic. Thermal fluctuations in principle can be incorporated to study a wider range of applications; however, we use molecular dynamics in part because one can incorporate geometric constraints in a straightforward manner.

III. MODEL PARAMETRIZATION

We want to evaluate the validity of using a collection of discrete Stokeslets to approximate the behavior of a continuous filament. Relevant analytical solutions that can be used for comparison are numbered and only manageable in the regime of small deformation. Our comparisons to theoretical results are likewise restricted to this regime. Cox, Batchelor, and Tillet carried out seminal theoretical work on a slender elastic body undergoing sedimentation with which some comparisons can be made [30–32]. In this section, we parametrize our model specifically to recover their theoretical results. We discuss how the methodology can be generalized to match other expressions in Sec. V.

A. Collective friction coefficients

Take the example of a filament experiencing a uniform external force density perpendicular to its axis denoted by $f^y(=F_j^y/b)$. Equation (7) for this example is

$$F_{iH} = -\gamma_0^{\perp}v_i + \frac{3a^{\perp}f^y}{4}\left(\sum_{j=1}^{i-1}\frac{1}{j} + \sum_{j=1}^{n-i}\frac{1}{j}\right). \tag{12}$$

The sum in Eq. (12) can be estimated using the definition of the Euler-Mascheroni constant, $k(\approx 0.5772)$,

$$k = \lim_{m\to\infty}\left[\sum_{j=1}^{m}\frac{1}{j} - \ln(m)\right]. \tag{13}$$

Although this definition is for an infinite series, the following finite sum is a good approximation:

$$\sum_{j=1}^{m}\frac{1}{j} \approx \ln(m) + k. \tag{14}$$

For instance, for $m=100$, the highest order omitted term $(1/2m)$ in the harmonic series is already two orders of magnitude smaller than k. With this approximation, we can write Eq. (12) in terms of the dimensionless contour length, $x[=-1+(i-1)(b/l)]$, spanning the interval $[-1,1]$. The result is

$$F_H(x) = -\gamma_0^{\perp}v(x) + \frac{3a^{\perp}f^y}{4}\ln\left(\frac{1-x^2}{(\beta b/l)^2}\right), \tag{15}$$

where $\beta = e^{-k}$.

Consider the steady-state solution, when the total hydrodynamic force matches the external force ($-F^y = F_H$). All sections of the filament move with the same velocity, the terminal or steady-state velocity, which we label U. Using $L \approx nb$ for large n, we have

$$-bf^y = -\gamma_0^\perp U + \frac{1}{L}\int_{-1}^{1}\left[\frac{3a^\perp f^y}{4}\left\{\ln\left[\frac{1-x^2}{(\beta b/l)^2}\right]\right\}\right]dx. \tag{16}$$

The logarithmic term diverges at the ends but is integrable. The solution is

$$\gamma_0^\perp U = F^y\left\{\frac{b}{L} + \frac{3a^\perp}{2L}\left[\ln\left(\frac{L}{\beta b}\right) - 1\right]\right\}. \tag{17}$$

The collective friction coefficient ($\gamma^\perp$) of a sedimenting filament can be evaluated by taking the quotient of the total imposed external force and the resultant terminal velocity,

$$\gamma^\perp = \frac{F^y}{U} = \frac{4\pi\eta L}{\ln[L/(\beta b)] + \frac{2b}{3a^\perp} - 1}. \tag{18}$$

From theory [30], the friction coefficient of a slender body is

$$\bar{\gamma}^\perp = \frac{4\pi\eta L}{\ln(L/r) + C_2} + O[\ln^{-3}(L/r)], \tag{19}$$

where C_2 depends on the cross-sectional shape. For a uniform circular cross section $C_2 = \ln(2) - 1/2$. When the filament radius is chosen to be $r/b = \beta \approx 0.562$ and the hydrodynamic radius is chosen to be $a^\perp/b = 4/[3(2\ln 2 + 1)] \approx 0.559$, our result is in agreement with theory (to the order of error in the equations) for the case of sedimentation perpendicular to the axis.

Starting with Eq. (7) and instead considering the scenario of the filament experiencing a uniform force density parallel to its axis, we find that the collective friction coefficient is

$$\gamma^\parallel = \frac{2\pi\eta L}{\ln[L/(\beta b)] + \frac{b}{3a^\parallel} - 1}. \tag{20}$$

From theory,

$$\bar{\gamma}^\parallel = \frac{2\pi\eta L}{\ln(L/r) + C_1} + O[\ln^{-3}(L/r)], \tag{21}$$

where C_1 is a coefficient that again depends on the cross-sectional shape. For a uniform circular cross section, $C_1 = \ln(2) - 3/2$. For the case of axial sedimentation, our results match theory when $r/b = \beta \approx 0.562$ and $a^\parallel/b = 2/[3(2\ln 2 - 1)] \approx 1.73$.

B. Relationships between *a*, *r*, and *b*

In order for the Stokesian hydrodynamic treatment to be consistent with the results from slender body theory, the hydrodynamic and the filament radii must be chosen appropriately. In the shish kebab model both a and r are chosen to be simply $b/2$ [17]. However, our analysis indicates that there is a more consistent choice.

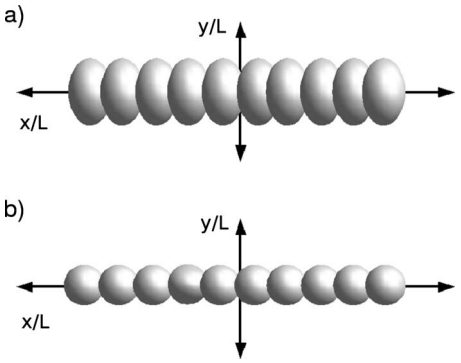

FIG. 1. A schematic of the friction strength using the (a) caterpillar and (b) shish kebab models.

First, we determined that when the filament radius using the Stokesian treatment is considered to be $r/b = \beta$, it is dependent on the degree of discretization [33]. As the discretization increases, the bead spacing decreases and the model mimics a more slender filament. The more interesting result is that two hydrodynamic radii are required to recover the correct dynamic behavior in both the perpendicular and parallel directions. In studies using resistive force theory [Eq. (8)], a popular choice for the ratio of the *bead* friction coefficients is $\gamma_0^\parallel/\gamma_0^\perp = 0.5$ equivalent to the ratio of the *collective* friction coefficients in the limit of an infinitely slender body. In our model, which includes filament-fluid coupling, the ratio of the bead friction coefficients is $\gamma_0^\parallel/\gamma_0^\perp \approx 3.09$. This is counterintuitive because the collective parallel friction coefficient of the filament is actually always lower than the perpendicular. But, as we will show in Sec. IV, the friction coefficients for collective filament motion in each direction are recovered to a greater degree of accuracy using these values.

Given the effective radius for parallel movement is around three times that for perpendicular movement, the resultant hydrodynamic shape of the filament is caterpillarlike having the basic features of an ordinary garden cabbage looper. Therefore, we refer to it as "caterpillar" Oseen hydrodynamics. An illustration of the hydrodynamic shape is shown in Fig. 1.

C. Inhomogeneous hydrodynamic force

As a further confirmation that our results are consistent, there is an additional theoretical result with which we can compare: the (inhomogeneous) friction coefficient along the contour length during sedimentation [30,34]. The result for perpendicular sedimentation, rewritten in terms of the variable definitions in this paper, is

$$\frac{f^y}{2\pi\eta U} = -\frac{2}{\ln(\epsilon)} - \frac{1 + 2\ln(2) + \ln(1-x^2)}{\ln^2(\epsilon)} + O[\ln^{-3}(\epsilon)], \tag{22}$$

where the constant ϵ is the *slenderness parameter* defined as $\epsilon = r/l$.

Defining $\tilde{\epsilon} = \beta b/l$, we can write the steady-state friction from Eq. (15) as

$$\gamma_0^{\perp} U = bf^y + \frac{3a^{\perp} f^y}{4} \ln\left(\frac{1-x^2}{\tilde{\epsilon}^2}\right). \tag{23}$$

We expand Eq. (23) in terms of $\ln^{-1}(\tilde{\epsilon})$ to get

$$\frac{f^y}{2\pi\eta U} = -\frac{2}{\ln(\tilde{\epsilon})} - \frac{\frac{4b}{3a^{\perp}} + \ln(1-x^2)}{\ln^2(\tilde{\epsilon})} + O[\ln^{-3}(\tilde{\epsilon})]. \tag{24}$$

This is equivalent to Eq. (22) when the following two conditions hold:

$$\tilde{\epsilon} = \epsilon, \tag{25}$$

$$\frac{a^{\perp}}{b} = \frac{4}{3[2\ln(2)+1]}. \tag{26}$$

Therefore, the filament radius is $r/b = \beta$ and the effective hydrodynamic radius is $a^{\perp}/b = 4/[3(2\ln 2+1)]$. The analysis also holds for a comparison of the hydrodynamic force during parallel sedimentation.

These conclusions are consistent with those from the analysis in Sec. III A, where we calculated the collective friction coefficient for sedimentation in the perpendicular direction. Confirmation that the correct inhomogeneous hydrodynamic force is recovered, even while neglecting higher-order terms in Eq. (19), is significant since it is this variation in the hydrodynamic force that causes the deformation of the flexible body.

IV. RESULTS FROM SIMULATION

To compare our computational model with slender body theory, a series of simulations was carried out. For all calculations, the starting configuration is a single filament oriented along the x axis. The number of beads n (and the resultant filament slenderness) in this case is variable. Each pair of neighboring beads is constrained to be at a separation $b = L/(n-1)$. The velocity was initialized to zero. We introduce a dimensionless force

$$B = \frac{L^3 F}{\alpha}, \tag{27}$$

which weighs the relative magnitudes of the elastic and external forces. When $B \ll 1$, elastic forces dominate and the filament remains largely straight. When $B \gg 1$, the magnitude of the external forces is large enough for significant deformation to occur.

The test case we consider is a full dynamic simulation of sedimentation, both parallel and perpendicular to the primary axis of the filament. A uniform force density was applied to the system and the equations of motion integrated until the body reached a constant terminal velocity. From this steady-state configuration, we analyzed the forces. To give an idea of the computational cost, a typical simulation of a filament modeled with 80 beads takes less than 1 h on a computer with an Intel Pentium D processor (3.00 GHz) running Fedora Linux. To allow comparison with theory the magnitudes of the external force density and the flexure were chosen such that the deflection amplitude is small (well within 1% of the length) in the steady-state configuration. In terms of the dimensionless force, all simulations were carried out with $B \leq 0.01$. For the model this is not a necessary restriction; the high B regime can also be studied. The length L for all simulations was set to unity.

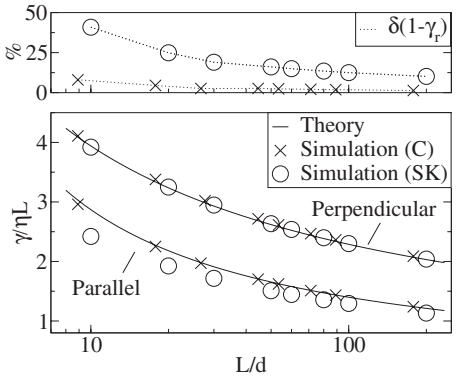

FIG. 2. Bottom: simulation results for the collective friction coefficient versus aspect ratio of a sedimenting filament in steady state using caterpillar (C) and shish kebab (SK) parametrizations. Slender body theory expressions are included for comparison. Top: relative error in $(1-\gamma_r)$, where $\gamma_r = \gamma^{\parallel}/\gamma^{\perp}$.

The collective friction coefficients calculated from our simulations are plotted in Fig. 2 along with the theoretical values from Eqs. (19) and (21). Our model shows excellent agreement to theory even for the very smallest aspect ratio. In contrast, calculations using the shish kebab parametrization do not. The values for the case of sedimentation perpendicular to the axis are reproduced accurately because the hydrodynamic radius is chosen to be $a/b = 1/2$, which is very close to our value of $a^{\perp}/b = 0.559$. The collective friction coefficient that results from motion parallel to the axis, however, only matches in the limit that the body is infinitely slender. The results in the limit of a moderate cross section $(L/d \approx 50)$ differ significantly from theory. The discrepancy is over 15% for the lowest aspect ratio considered.

We can also compare the inhomogeneous friction coefficient as a function of contour length that was introduced in Sec. III C. We include this comparison for completeness even though we expect the simulation results from the caterpillar and shish kebab models to be quantitatively similar given that only perpendicular motion is considered for this scenario. The theoretical expression [Eq. (22)] and results from simulation are plotted in Fig. 3. Both the caterpillar and shish kebab parametrizations show excellent agreement overall, although the deviation from theory is minimized when using a tensor hydrodynamic radius. The slight deviation is due to the fact that we are comparing our model to only the leading order term from theory, although our simulation results contain higher-order contributions. The higher-order terms appear to have little cumulative effect on the collective friction coefficient results in Fig. 2.

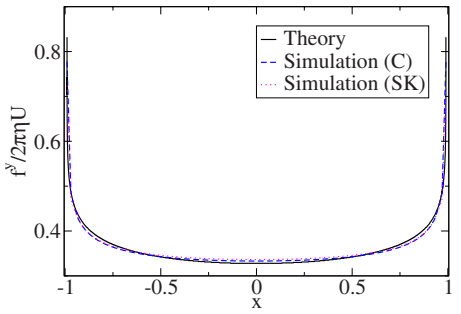

FIG. 3. (Color online) The variation in the friction as a function of contour length from theory and from simulations using caterpillar (C) and shish kebab (SK) parametrization ($n=100$, $B=0.01$).

Xu and Nadim extended the groundwork of Cox, Batchelor, and Tillett and determined an expression for the y deflection by solving the differential equation of beam deflection from elasticity theory by using the appropriate Green's function [13]. From Eq. (7) in their article, the deflection is given by

$$y(x) = -\frac{C}{24}\left[(1+x)^4\ln(1+x) + (1-x)^4\ln(1-x) - \left(\frac{13}{6} + 2\ln 2\right)x^4 - (1+12\ln 2)x^2\right]. \quad (28)$$

Please note that there is a typographical error in the original paper that has been corrected here [35]. The constant C is

$$C = \frac{2\pi\eta U l^4}{EI\ln^2(\epsilon)}, \quad (29)$$

where EI is the Young's modulus times the second moment of area, which together constitute the beam flexure α. The ranges of the parameters for which the deflection was calculated are $B=10^{-5}-10^{-1}$ and $L/d\approx 20-400$. All parameter sets investigated yielded the same dimensionless deflection. Two representative data sets are plotted in Fig. 4. Using the caterpillar model, when the theoretical dimensionless deflection is scaled by a constant factor of approximately 1.15, the theory matches our simulation. The scaling factor is 1.14 using the shish kebab model. The minor quantitative discrepancy could be due to the fact that the theoretical deflection [Eq. (28)] is calculated from a differential equation that does not include a Lagrange multiplier to impose constant length.

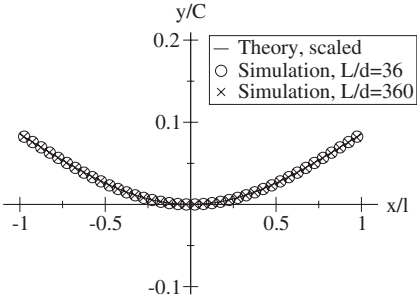

FIG. 4. Dimensionless deflection as a function of contour length.

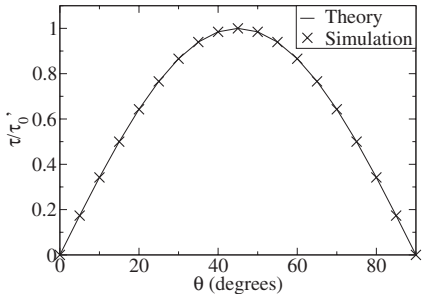

FIG. 5. Normalized torque as a function of θ, the angle between the filament end-to-end vector, and the plane orthogonal to the force axis.

In this way, our simulation model is a slightly different description. No extension whatsoever can be accommodated in the axial direction. It is significant to note that both the theoretical and simulation results agree in the prediction that the functional form of the deflection is independent of slenderness.

Xu *et al.* also derived an expression for the torque acting on a flexible slender body. The torque will cause the filament to rotate during sedimentation until a final orientation is achieved in which the filament's centerline is perpendicular to the force axis. Their result is

$$T = C_T\frac{2\pi^2\eta^2U^2l^5\sin(2\theta)}{EI\ln^4(\epsilon)} = \tau_0\sin(2\theta). \quad (30)$$

The variable θ is the angle between the filament axis and $\hat{x}$ when the external force is applied in the $\hat{y}$ direction. C_T is

$$C_T = \int_0^1 y(x)[2\ln 2 - 2 - \ln(1-x^2)]dx \approx 0.016\,61 \quad (31)$$

calculated by numerical integration. The normalized torque as a function of θ is plotted in Fig. 5 along with the theoretical functional dependence. For the functional forms the results are in excellent agreement. However, the normalization constant τ_0' from Fig. 5 is different from τ_0 from theory. This is expected since the y deflection from our simulation results differs slightly from the analytic result that was used in the derivation of Eq. (30). Simulation results of the normalized torque were quantitatively equivalent using both the caterpillar and shish kebab parametrizations, but the normalization constant τ_0' differed.

V. DISCUSSION AND CONCLUSIONS

We described a simulation model for an elastic filament that accurately accounts for intrafilament hydrodynamic interactions. We showed that the discrete Stokesian treatment encapsulates the physics of a continuous filament of finite cross section when a specific tensor bead friction is chosen without the need for an explicit surface. Furthermore, in the

limit that the inhomogeneity in the friction coefficient is neglected, the caterpillar model reduces to simple resistive force theory with a tensor bead friction coefficient. It follows from our analysis that the bead spacing dictates the local radius of the filament. Therefore, when the two consecutive beads are not constrained but instead connected by a simple spring, the interbead distance and, therefore, the resultant filament radius is variable [15,16]. By applying length constraints to the interbead distance, as we do in this model, the radius is constant along the contour length of the filament.

The caterpillar model accurately simulates the dynamics of filament sedimentation for all aspect ratios considered, whereas the shish kebab parametrization only recovers the correct collective friction coefficients for an infinitely slender body (infinitely high bead density). A filament in nature may have a diameter a few percent of the filament length [1–3]. There is significant deviation from the correct hydrodynamic behavior in this regime using the shish kebab parametrization, which may be nontrivial. The ratio of the two friction coefficients is particularly important in the field of microorganism motility. The swimming speed (and thrust) of an activated filament, for instance, is proportional to $(1-\gamma^{\parallel}/\gamma^{\perp})$ [2]. Any deviation in this ratio will have significant effects on the motility. We plotted the relative error in this quantity in the top graph of Fig. 2. For an aspect ratio of $L/d \approx 1/50$, the error is 16% and 2% for the shish kebab and caterpillar models, respectively. Furthermore, the reorientation times of a filament in a uniform external field in Ref. [12] differ by 30% for the shish kebab and caterpillar models. Although one would reach the same general conclusions for scaling behavior using either parametrization, the onset of the observation of the metastable "W"-shape state in their studies would likely be appreciably affected. Whether a tensor hydrodynamic radius is necessary should be evaluated on a case-by-case basis.

Our simulation results for the dimensionless deflection of a filament sedimenting perpendicular to its axis agree with the theoretical prediction that the steady-state shape does not depend on the slenderness of the filament. Also, calculations of the torque acting on a misaligned filament support that the functional dependence is $\sin(2\theta)$. We observed a modest discrepancy in the magnitude of the dimensionless deflection between our simulations and the theoretical results. A potential source of the difference may be that the theoretical deflection is calculated from a differential equation that does not explicitly include a Lagrange multiplier to enforce constant length, whereas our simulation model does not accommodate any degree of axial extension.

We have chosen the hydrodynamic radius specifically to recover the results of a body with a uniform circular cross section. But, it is possible to choose it instead to match the collective parallel and perpendicular friction coefficients for a different cross-sectional radius profile [30]. One simply has to use different values for the constants C_2 and C_1 in Eqs. (19) and (21), respectively. This means that the dynamic response actually depends on the specific geometry considered. We chose a uniform circular cross section because it is a commonly used starting point for the shape of microtubules, nanotubes, cilia/flagella, and fabricated filament-based microswimmers.

The methodology we present here can be further generalized in two important ways. First, we have chosen r, $a^{\perp}$, and $a^{\parallel}$ specifically to match expressions from slender body theory; however, as the filament approaches an aspect ratio of unity, the body is no longer slender and these equations are no longer valid. For very thick filaments, one could instead match to more accurate numerical results. We successfully applied our methodology to the numerical expressions listed in Ref. [36] relevant for aspect ratios of $L/d \approx 2-30$. Specifically, we equate our Eqs. (18) and (20) to their corresponding numerically derived expressions for the friction coefficients to determine optimal values for the hydrodynamic radii. Please see Ref. [37]. Using these values, we can report that agreement between simulations and the expressions in Ref. [36] is quantitatively similar to that shown in Fig. 2 using the original parametrization with slender body theory as the reference point. This analysis demonstrates a significant numerical advantage. Namely, that for an equivalent number of beads (i.e., computational expense) one can parametrize the same model/description to get two different physical limits: the slender limit or the "thick" limit.

Second, the model can be extended beyond Oseen hydrodynamics. The Oseen tensor is accurate in the far field but diverges for two spheres that overlap. The Rotne-Prager (RP) tensor is a higher-order description that is widely used because it reduces the error due to singularities of two beads that closely approach [38]. For a single filament simulation, however, this point is mute. The beads are constrained to be a specific separation apart. Also, the model is specifically for a filament whose length is well below its persistence length rendering the risk of overlap nonexistent unless there is an exceptionally high external field. Only if one is considering a system with more than one filament must one worry about overlap. In this case, it is possible to apply caterpillar methodology to simulations using the RP tensor. Using the RP tensor, we went through the same analysis described in Sec. III A to determine expressions for r, $a^{\perp}$, and $a^{\parallel}$. Results are quoted in Ref. [39]. Since the RP tensor is not the next term in a systematic expansion of the hydrodynamic flow due to a force distributed on a cylinder, there is no reason to necessarily expect a numerical improvement in the friction coefficients with respect to the Oseen tensor. Indeed, we found that for single filament simulations, it is advantageous to use Oseen hydrodynamics because one can recover friction coefficients to a marginally higher degree of accuracy at a reduced computational expense (roughly a factor of 1/2). However, if the dynamics of multiple filaments are being investigated and collision is likely, the RP tensor with the parameters given in Ref. [39] can be used to prevent error due to singularities from overlap while still improving the dynamic behavior compared to using a scalar bead friction.

Elastic, hydrodynamic, and tension forces form the basis for the model. However, incorporating other forces is trivial. Biological molecules are frequently charged. With this model, one could investigate the dynamics of a charged filament such as a microtubule in an electric field, for example

[6,7]. The scope of problems one can investigate using the deterministic simulation model presented here, in which thermal fluctuations are neglected, is delineated by the condition that the time scale of diffusion is significantly longer than the time scale associated with the motion of interest. In practice this restricts its applicability to relatively stiff filaments. Nonetheless, similar considerations of parametrizing the Stokeslet hydrodynamic description apply when one includes thermal fluctuations. Such a model can then address an even wider class of important problems notably the dynamics of DNA fragments.

ACKNOWLEDGMENTS

We thank Professor A. Nadim for helpful discussions. A.G.B. thanks the Thouron Foundation, NSF, and the Thomas Young Centre for support. I.P. acknowledges financial support from MICINN (Project No. FIS2008-04386).

[1] E. M. Purcell, Am. J. Phys. **45**, 3 (1977).
[2] C. Brennen and H. Winet, Annu. Rev. Fluid Mech. **9**, 339 (1977).
[3] G. J. Hancock, Proc. R. Soc. London, Ser. A **217**, 96 (1953).
[4] D. Smith, E. Gaffney, and J. Blake, Bull. Math. Biol. **69**, 1477 (2007).
[5] R. Dreyfus, J. Baudry, M. Roper, M. Fermigier, H. Stone, and J. Bibette, Nature (London) **437**, 862 (2005).
[6] M. van den Heuvel, M. de Graaff, S. Lemay, and C. Dekker, Proc. Natl. Acad. Sci. U.S.A. **104**, 7770 (2007).
[7] M. G. L. van den Heuvel, R. Bondesan, M. Cosentino Lagomarsino, and C. Dekker, Phys. Rev. Lett. **101**, 118301 (2008).
[8] C. P. Lowe, Philos. Trans. R. Soc. London, Ser. B **358**, 1543 (2003).
[9] G. P. Alexander, C. M. Pooley, and J. M. Yeomans, Phys. Rev. E **78**, 045302(R) (2008).
[10] I. Llopis, I. Pagonabarraga, M. Cosentino Lagomarsino, and C. P. Lowe, Phys. Rev. E **76**, 061901 (2007).
[11] J. Gray and G. J. Hancock, J. Exp. Biol. **32**, 802 (1955).
[12] M. Cosentino Lagomarsino, I. Pagonabarraga, and C. P. Lowe, Phys. Rev. Lett. **94**, 148104 (2005).
[13] X. Xu and A. Nadim, Phys. Fluids **6**, 2889 (1994).
[14] M. J. Shelley and T. Ueda, Physica D **146**, 221 (2000).
[15] Y. W. Kim and R. R. Netz, Phys. Rev. Lett. **96**, 158101 (2006).
[16] X. Schlagberger and R. R. Netz, Phys. Rev. Lett. **98**, 128301 (2007).
[17] M. Doi and S. F. Edwards, *The Theory of Polymer Dynamics* (Oxford University Press, Oxford, UK, 1986).
[18] L. Landau and E. Lifshitz, *Theory of Elasticity*, 3rd ed. (Butterworth-Heinemann, Boston, MA, 1986).
[19] O. Kratky and G. Porod, Recl. Trav. Chim. Pays-Bas **68**, 1106 (1949).
[20] M. Fixman and J. Kovac, J. Chem. Phys. **58**, 1564 (1973).
[21] S. B. Smith, L. Finzi, and C. Bustamante, Science **258**, 1122 (1992).
[22] J. Marko and E. Siggia, Macromolecules **28**, 8759 (1995).
[23] J.-P. Ryckaert, G. Ciccotti, and H. J. C. Berendsen, J. Comput. Phys. **23**, 327 (1977).
[24] A. G. Bailey, C. P. Lowe, and A. P. Sutton, J. Comput. Phys. **227**, 8949 (2008).
[25] W. C. Swope, H. C. Andersen, P. H. Berens, and K. R. Wilson, J. Chem. Phys. **76**, 637 (1982).
[26] M. Tuckerman, B. J. Berne, and G. J. Martyna, J. Chem. Phys. **97**, 1990 (1992).
[27] G. Kalibaeva, M. Ferrario, and G. Ciccotti, Mol. Phys. **101**, 765 (2003).
[28] R. Argentini, Ph.D. thesis, Universiteit van Amsterdam, 2008.
[29] C. P. Lowe, FGCS, Future Gener. Comput. Syst. **17**, 853 (2001).
[30] R. G. Cox, J. Fluid Mech. **44**, 791 (1970).
[31] G. K. Batchelor, J. Fluid Mech. **44**, 419 (1970).
[32] P. K. Tillett, J. Fluid Mech. **44**, 401 (1970).
[33] Alternatively, for a given bead spacing b, we can dictate the aspect ratio by introducing a scaling factor δ and by using the more general equations $r/b=\delta\beta$, $a^{\perp}/b=4/\{3[2\ln(2/\delta)+1]\}$, and $a^{\parallel}/b=2/\{3[2\ln(2/\delta)-1]\}$. Solutions exist for $\delta<1.21$. This corresponds to the condition that r/b must be less than 0.681. This is a useful result in that for a specified bead number, one can simulate a filament of a given slenderness at an equivalent computational expense.
[34] J. B. Keller and S. I. Rubinow, J. Fluid Mech. **75**, 705 (1976).
[35] We are grateful to Professor A. Nadim for pointing this out to us.
[36] M. Tirado, C. Martinez, and J. de la Torre, J. Chem. Phys. **81**, 2047 (1984).
[37] The resultant parametrization is $a^{\perp}/b=2/[3(-\ln 2+0.839+0.185/p+0.233/p^2+1)]$ and $a^{\parallel}/b=1/[3(-\ln 2-0.207+0.980/p-0.133/p^2+1)]$ with $r/b=\beta$, where $L/d=p$ for the parametrization.
[38] J. Rotne and S. Prager, J. Chem. Phys. **50**, 4831 (1969).
[39] We calculated the parametrization to match slender body theory using the RP tensor to be $a^{\perp}/b\approx 0.559$ and $a^{\parallel}/b\approx 0.441$, with $r/b\approx 0.437$.